

Structural and transport properties of $(Mg,Fe)SiO_3$ at high temperature and high pressure

Shu Huang(黄澍), Zhiyang Xiang(向志洋), Shi He(何适), Luhan Yin(尹路寒), Shihe Zhang(张时赫), Chen Chen(陈晨), Kaihua He(何开华), and Cheng Lu(卢成)

Citation: Chin. Phys. B, 2025, 34 (**3**): 036102. DOI: 10.1088/1674-1056/ada759
Journal homepage: http://cpb.iphy.ac.cn; http://iopscience.iop.org/cpb

What follows is a list of articles you may be interested in

Effect of Mn element on shock response in $CoCrFeNiMn_x$ high entropy alloys

Peng Wen(闻鹏), Changxing Du(杜长星), Gang Tao(陶钢), and Guipeng Ding(丁贵鹏)
Chin. Phys. B, 2024, 33 (**11**): 116103. DOI: 10.1088/1674-1056/ad7fd0

Quasi-plastic deformation mechanisms and inverse Hall-Petch relationship in nanocrystalline boron carbide under compression

Zhen Yue(岳珍), Jun Li(李君), Lisheng Liu(刘立胜), and Hai Mei(梅海)
Chin. Phys. B, 2024, 33 (**8**): 086105. DOI: 10.1088/1674-1056/ad4989

Properties of radiation defects and threshold energy of displacement in zirconium hydride obtained by new deep-learning potential

Xi Wang(王玺), Meng Tang(唐孟), Ming-Xuan Jiang(蒋明璇), Yang-Chun Chen(陈阳春), Zhi-Xiao Liu(刘智骁), and Hui-Qiu Deng(邓辉球)
Chin. Phys. B, 2024, 33 (**7**): 076103. DOI: 10.1088/1674-1056/ad362b

Effect of Y element on atomic structure, glass forming ability, and magnetic properties of FeBC alloy

Jin-Hua Xiao(肖晋桦), Da-Wei Ding(丁大伟), Lin Li(李琳), Yi-Tao Sun(孙奕韬), Mao-Zhi Li(李茂枝), and Wei-Hua Wang(汪卫华)
Chin. Phys. B, 2024, 33 (**7**): 076101. DOI: 10.1088/1674-1056/ad3dd4

Controlled thermally-driven mass transport in carbon nanotubes using carbon hoops

Yaolong Li(李耀隆), Songyuan Li(李松远), Meifen Wang(王美芬), and Renliang Zhang(张任良)
Chin. Phys. B, 2024, 33 (**4**): 046101. DOI: 10.1088/1674-1056/ad14ff

---

SPECIAL TOPIC — Structures and properties of materials under high pressure

Structural and transport properties of $(Mg,Fe)SiO_3$ at high temperature and high pressure

Shu Huang(黄澍)[1], Zhiyang Xiang(向志洋)[1], Shi He(何适)[1,2], Luhan Yin(尹路寒)[1], Shihe Zhang(张时赫)[1,3], Chen Chen(陈晨)[1], Kaihua He(何开华)[1], and Cheng Lu(卢成)[1,†]

[1] *School of Mathematics and Physics, China University of Geosciences (Wuhan), Wuhan* 430074, *China*
[2] *Faculty of Materials Science and Chemistry, China University of Geosciences (Wuhan), Wuhan* 430074, *China*
[3] *School of Future Technology, China University of Geosciences (Wuhan), Wuhan* 430074, *China*

(Received 11 December 2024; revised manuscript received 4 January 2025; accepted manuscript online 8 January 2025)

$(Mg,Fe)SiO_3$ is primarily located in the mantle and has a substantial impact on geophysical and geochemical processes. Here, we employ molecular dynamics simulations to investigate the structural and transport properties of $(Mg,Fe)SiO_3$ with varying iron contents at temperatures up to 5000 K and pressures up to 135 GPa. We thoroughly examine the effects of pressure, temperature, and iron content on the bond lengths, coordination numbers, viscosities, and electrical conductivities of $(Mg,Fe)SiO_3$. Our calculations indicate that the increase of pressure leads to the shortening of the O–O and Mg–O bond lengths, while the Si–O bond lengths exhibit the initial increase with pressure up to 40 GPa, after which they are almost unchanged. The coordination numbers of Si transition from four-fold to six-fold and eventually reach eight-fold coordination at 135 GPa. The enhanced pressure causes the decrease of the diffusion coefficients and the increase of the viscosities of $(Mg,Fe)SiO_3$. The increased temperatures slightly decrease the coordination numbers and viscosities, as well as obviously increase the diffusion coefficients and electrical conductivities of $(Mg,Fe)SiO_3$. Additionally, iron doping facilitates the diffusion of Si and O, reduces the viscosities, and enhances the electrical conductivities of $(Mg,Fe)SiO_3$. These findings advance fundamental understanding of the structural and transport properties of $(Mg,Fe)SiO_3$ under high temperature and high pressure, which provide novel insights for unraveling the complexities of geological processes within the Earth's mantle.

Keywords: $(Mg,Fe)SiO_3$, structural and transport properties, molecular dynamics simulations, high temperature and high pressure

PACS: 61.20.Ja, 61.50.Ks, 66.30.Pa, 66.20.Cy

DOI: 10.1088/1674-1056/ada759 **CSTR:** 32038.14.CPB.ada759

1. Introduction

$(Mg,Fe)SiO_3$, particularly the silicate perovskites and their high-pressure phases, play a crucial role in understanding the composition, structure, and dynamics of the Earth's mantle.[1–3] These minerals are predominant in the lower mantle, where they constitute a significant fraction of the Earth's mass.[4–7] Their presence and dynamic behavior under extreme conditions have profound implications for various geophysical and geochemical processes.[8–10] Normally, $(Mg,Fe)SiO_3$ is stabilized into denser crystal structure with orthorhombic *Cmcm* symmetry.[11–13] It undergoes several structural phase transitions at high temperature and high pressure.[14,15] For example, the structural transition of $(Mg,Fe)SiO_3$ from perovskite to post-perovskite occurs at Earth's lower mantle.[16] This transition accompanies the changes of the physical properties, such as density, viscosity, thermal and electrical conductivities of $(Mg,Fe)SiO_3$, which are crucial for modeling the Earth's interior processes.[17–23] Improved knowledge of these properties will help in interpreting seismic data, understanding the mechanisms behind mantle plumes, and predicting the behavior of mantle materials during subduction and upwelling processes. Moreover, $(Mg,Fe)SiO_3$ are also significant in the context of geochemical processes, including the cycling of elements such as magnesium, iron, and silicon.[24–26] Their interactions with melts and fluids in the mantle can influence the formation of magma, the generation of volcanic eruption, and the composition of volcanic substance.[27–29]

Recent advancements have been achieved in the exploration of the structural and transport properties of $(Mg,Fe)SiO_3$ under high temperature and high pressure. For instance, Mosenfelder *et al*. conducted shock loading experiments to elucidate the equation of state (EOS) of $MgSiO_3$, discovering various phases ranging from low-density glass to high-density perovskite and majorite.[18] Holzapfel *et al*. measured the Fe–Mg interdiffusion coefficients of $(Mg,Fe)SiO_3$ at pressures of 22–26 GPa and temperatures of 1973–2273 K, demonstrating extremely low diffusion rates.[30] Their results suggest that chemical equilibrium in the deep mantle is only attainable under conditions of significant deformation. Kavner

†Corresponding author. E-mail: lucheng@calypso.cn

© 2025 Chinese Physical Society and IOP Publishing Ltd. All rights, including for text and data mining, AI training, and similar technologies, are reserved.

et al. investigated the electrical conductivity of majorite at room temperature, inferring that the presence of both majorite and spinel phases may contribute to the observed increase in electrical conductivity from the upper mantle to the transition zone.[31] Chen *et al*. measured the viscosity of the SiO_2–FeO–MgO system in equilibrium with metallic Fe, revealing that substituting FeO with MgO results in increased viscosity and activation energy of the system.[32] Wan *et al*. employed *ab initio* molecular dynamics simulations to determine the diffusion coefficients and shear viscosities of molten $MgSiO_3$ under varying thermodynamic conditions. Their results indicated that the density of the melt was lower than that of the corresponding solid phase under core–mantle boundary conditions.[33] These findings are pivotal for understanding the structural, compositional, and dynamic properties of the mantle. However, experimental data on the transport properties of (Mg,Fe)SiO_3, including viscosity and electrical conductivity across the full mantle pressure range (up to 136 GPa), remain limited. Moreover, some experimental results regarding the pressure dependence of viscosities, particularly for silicate melts, are conflicting.[14–16] Most experimental studies have been restricted to lower pressure ranges (< 13 GPa), with only a few extending their measurements to 30 GPa.[17,21]

In contrast, molecular dynamics (MD) simulations provide significant computational efficiency, facilitating the simulation of larger systems and serving as a powerful methodology for examining the structural and transport properties of silicate melts[22,23] under high temperature and high pressure. In this work, we used the molecular dynamics simulations to study the structural and transport properties of (Mg,Fe)SiO_3 at high-temperature and high-pressure conditions up to 135 GPa and 5000 K. We assessed the effects of iron doping on the structural and transport properties of (Mg,Fe)SiO_3, specifically focusing on how varying iron concentrations influence the bond lengths, coordination numbers, viscosities, and electrical conductivities.

2. Methods

The classical MD simulations are conducted using the Large-scale Atomic/Molecular Massively Parallel Simulator (LAMMPS) software.[34] We choose a large scale (Mg,Fe)SiO_3 system containing about 5000 atoms with different concentrations of Fe dopants. The Verlet algorithm is employed to determine the motorial trajectories of the atoms, with a time step of 1 fs. The Ewald summation method is used to account for the long-range Coulomb interactions, and a uniform cut-off radius of 11.0 Å is adopted for both the long-range Coulomb and short-range interaction terms to balance the computational efficiency and accuracy. Temperature and pressure are controlled using the Nosé–Hoover thermostat and Nosé–Hoover barostat, respectively. The periodic boundary conditions (ppp) are applied throughout the simulation.[35–37] The initial configuration is generated by randomly distributing atoms within the simulation box, but atomic overlaps are prevented. The transport properties, such as viscosity, thermal conductivity, and self-diffusion coefficient are carried out in the canonical ensemble (NVT). The simulation durations are sufficiently long to ensure the convergences of the energies and forces.

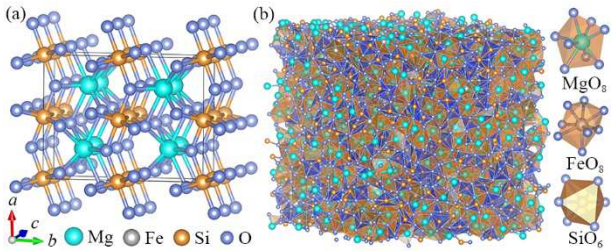


Fig. 1. (a) The crystal structure of the post-perovskite (pPv) phase of $MgSiO_3$. (b) The large-scale (Mg,Fe)SiO_3 at 5000 K and 135 GPa.

The selection of an appropriate potential function is crucial to ensuring the accuracy of MD simulations. Here, the van Beest–Kramer–van Santen (BKS) potential is employed, which has been proven to effectively describe the interatomic interactions in silicate minerals.[38] It is expressed as follows:

$$U_{ij}(r) = \frac{q_i q_j}{r_{ij}} + B_{ij}\exp(-r_{ij}/\rho_{ij}) - \frac{C_{ij}}{r_{ij}^6}, \tag{1}$$

where U_{ij} represents the potential energy between atoms, which is divided into three components. The first term is the long-range Coulomb interactions, where q_i and q_j are the charges of the ith and jth atoms, respectively. The second term is the short-range repulsive interactions, and the third term is the van der Waals interactions. The r_{ij} represents the distance between ith and jth atoms, while B_{ij} , ρ_{ij}, and C_{ij} are the potential parameters for each interaction term. To ensure the accuracy and efficiency of the MD simulations of silicate melts, we have used the potential parameters developed by Guillot *et al.*[39,40] Only the electrostatic interactions between cations are considered in the simulations due to that the interactions between oxygen ions and cations, as well as oxygen interionic interactions, are dominant the short-range interactions. The effective charges of the atoms are fixed, which are $-0.945e$, $0.945e$, $1.89e$, and $0.945e$ for O, Mg, Si and Fe ions, respectively. To explore the influence of iron content on the structural and transport properties of $(Mg_{1-x},Fe_x)SiO_3$ minerals, we have selected various concentrations of iron dopant with x values set to 0, 0.05, 0.10, and 0.15.

3. Results and discussion

3.1. Structure properties

At 2000 K, the O–O and Mg–O bond lengths of $MgSiO_3$ gradually decrease with increasing pressure, while the Si–O bond lengths increase with pressure up to 40 GPa, after which

it stabilizes at a constant value as pressure continues to rise. A similar behavior for the Si–O bond lengths of mantle rocks at pressures below 40 GPa was observed by Solomatova *et al.*[41] The Si–O bond length is 1.64 Å at 2000 K and ambient pressure, which is in good agreement with our calculations, indicating that our computational method is reliable. For $Mg_{0.9}Fe_{0.1}SiO_3$ at 4000 K, the O–O bond lengths decrease from 2.673 Å at 0 GPa to 2.365 Å at 135 GPa, while the Mg–O bond lengths contract from 1.969 Å to 1.881 Å. In contrast, the Si–O bond lengths remain relatively stable, ranging from 1.617 Å to 1.639 Å, and the Fe–O bond lengths decrease gradually from 1.947 Å to 1.903 Å. At higher temperatures of 5000 K, the trends in bond length variations are similar, however, the Fe–O bond lengths exhibit a more pronounced reduction at the 10% doping. The Mg–O bond length shows a clear decreasing trend under different temperature and pressure conditions. At both 4000 K and 5000 K, the Mg–O bond lengths decrease with increasing pressure. At 4000 K, the Mg–O bond lengths decrease from 1.969 Å at 0 GPa to 1.881 Å at 135 GPa, indicating that the bond lengths between Mg and O atoms contract as the pressure increases. This trend remains consistent at higher temperatures.

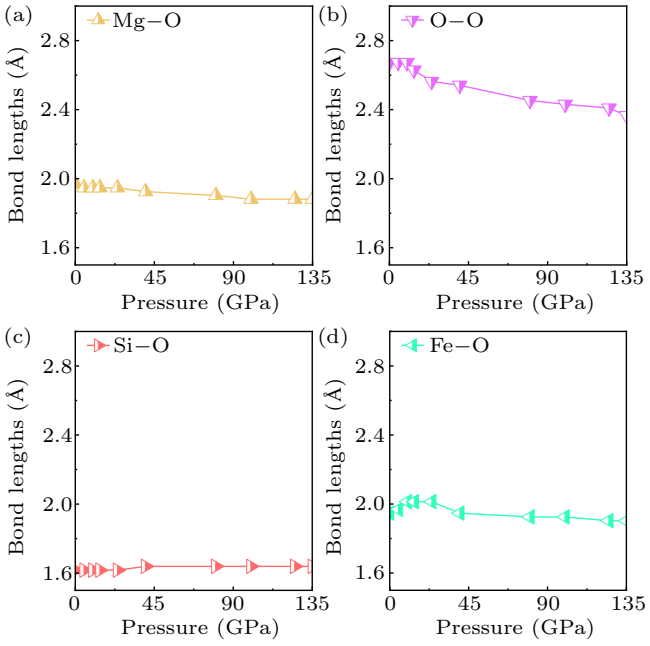


Fig. 2. The bond lengths in $Mg_{0.9}Fe_{0.1}SiO_3$ at 4000 K under different pressures. (a) Mg–O bond lengths, (b) O–O bond lengths, (c) Si–O bond lengths, and (d) Fe–O bond lengths.

The changes in O–O bond lengths are also evident. At 4000 K, the O–O bond length reduces from 2.673 Å at 0 GPa to 2.365 Å at 135 GPa. Unlike the Mg–O bonds, the contractions of the O–O bond lengths are slightly larger, especially under high pressure (e.g., at 135 GPa), where the O–O bond lengths decrease by about 0.3 Å compared to the initial O–O bond length of $Mg_{0.9}Fe_{0.1}SiO_3$ at 24 GPa. At higher temperatures, the changes in O–O bond lengths are similar. Although the initial O–O bond lengths at 0 GPa and 5000 K are slightly larger (2.695 Å), they also contract to 2.365 Å at 135 GPa. This indicates that increasing pressure decreases the distance between oxygen atoms, while rising temperature slightly alleviates this effect.

The Si–O bond lengths are relatively stable. Whether at 4000 K or 5000 K, the Si–O bond lengths remain around 1.639 Å, with only minor variations in conditions (e.g., at 40 GPa and 4000 K, the Si–O bond length is 1.639 Å). This indicates that over a wide range of temperatures and pressures, the Si–O bond length undergoes minimal change, suggesting that the Si–O bonds are robust and rigid chemical bonds that are less affected by changes in temperature or pressure. The Fe–O bond lengths exhibit more obvious changes, especially under high-temperature conditions. At 4000 K, the Fe–O bond lengths decrease from 1.947 Å at 0 GPa to 1.903 Å at 135 GPa, indicating a marked contraction of the Fe–O bond with increasing pressure. This contraction is also evident at higher temperatures. For instance, at 5000 K, the Fe–O bond lengths decrease from 1.859 Å at 0 GPa to 1.881 Å at 135 GPa. Notably, the effect of temperature on the Fe–O bond length is visible, with the Fe–O bond lengths at 5000 K being lower than those at 4000 K, indicating that the increase in temperature may lead to greater contraction of the Fe–O bonds compared to other chemical bonds. Overall, the $Mg_{0.9}Fe_{0.1}SiO_3$ exhibits a general trend of bond length contraction with increasing pressure, particularly for the Mg–O, O–O, and Fe–O bonds. The influence of temperature is minor on the Si–O bonds, while it is more pronounced for the Fe–O bonds.

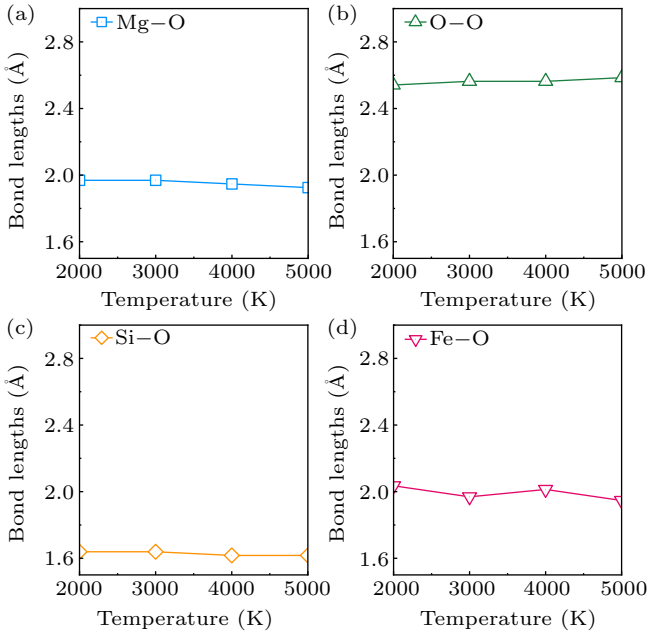


Fig. 3. The bond lengths in $Mg_{0.9}Fe_{0.1}SiO_3$ under 24 GPa at different temperatures. (a) Mg–O bond lengths, (b) O–O bond lengths, (c) Si–O bond lengths, and (d) Fe–O bond lengths.

We then discuss the average coordination numbers of Mg, Si, and Fe atoms in $Mg_{0.9}Fe_{0.1}SiO_3$ at different temperatures

and pressures. At 2000 K, the average coordination numbers of Si atoms in $Mg_{0.9}Fe_{0.1}SiO_3$ increase from 4.01 at 0 GPa to 6.0 at 135 GPa. Thus, the local structure of Si atoms at 0 GPa is dominated by four-coordinated Si–O tetrahedra. As the pressure increases to 24 GPa, six-coordinated Si–O octahedra become the dominant geometries, with the proportions of four-coordinated Si atoms gradually decreasing to about 3.1% at 40 GPa. At 80 GPa, the eight-coordinated Si–O polyhedra begin to emerge, indicating the increased densities in the melt and glass structures, as the proportions of four-coordinated Si atoms diminish to 0.4%. The coordination numbers of Mg atoms in $Mg_{0.9}Fe_{0.1}SiO_3$ are different from those of Si atoms. The Mg atoms are mainly in six-coordinated states at low temperatures and pressures. At 0 GPa and 2000 K, the average coordination numbers of Mg atoms are about 5.31, with local structures primarily composed of five- and six-coordinated MgO_5 and MgO_6 polyhedra. As pressure increases, Mg atoms transition to six- and seven-coordinated states at 14 GPa. With pressure exceeding 100 GPa, Mg atoms mainly occupy seven- and eight-coordinated states, with an average coordination number of about 6.63 at 135 GPa. The coordination numbers of Mg atoms are consistently larger than those of Si atoms under the same conditions. In most cases, the coordination numbers of Fe atoms in $Mg_{0.9}Fe_{0.1}SiO_3$ are slightly lower than those of Mg atoms, exhibiting a similar coordination trend. For example, the coordination numbers of Fe atoms are about 5.13 at 0 GPa and 2000 K, compared to 5.31 for Mg atoms under the same conditions. The Fe atoms also undergo a transition from five-coordinated to higher coordination states with increasing pressure, reaching an average coordination number of approximately 6.49 at 135 GPa.

We also conduct detailed analyses of the coordination distributions of $Mg_{0.9}Fe_{0.1}SiO_3$ under different pressures. At 0 GPa, 89.8% of Si atoms in $Mg_{0.9}Fe_{0.1}SiO_3$ are four-coordinated, while 10.1% are five-coordinated. For Mg atoms, 18.57% are four-coordinated, 40.1% are five-coordinated, and 30.2% are six-coordinated. At 14 GPa, the four-, five-, and six-coordinated Si atoms account for 50.2%, 35.1%, and 14.7%, respectively. The six-, seven-, and eight-coordinated Mg atoms are present in proportions of 6.2%, 38.6%, and 14.4%. At 24 GPa, the four-, five-, and six-coordinated Si atoms are 17%, 39.3%, an 43.7%, while the five-, six-, and seven-coordinated Mg atoms are 3.6%, 29.2%, an 42.6%. At 135 GPa, the five-, six-, and seven-coordinated Si atoms are 7.8%, 83%, and 9%, and the six-, seven-, and eight-coordinated Mg atoms are 25.6%, 49%, and 21.9%, respectively.

In comparison to pure $MgSiO_3$, the addition of iron in $Mg_{0.9}Fe_{0.1}SiO_3$ significantly affects the coordination distribution of Si atoms. At lower pressures, the average coordination number of Si in $Mg_{0.9}Fe_{0.1}SiO_3$ is slightly higher than that in $MgSiO_3$, suggesting that the presence of iron enhances the polyhedral connectivity of Si–O bonds. As pressure increases, the presence of iron further promotes the formation of six- and eight-coordinated structures, accelerating the transition of Si coordination from four-fold to higher coordination states. This indicates that iron doping increases the density and degree of polymerization in the melt structure by altering the local environment of Si, leading to a substantial impact on the Si coordination.[42,43]

3.2. Transport properties

3.2.1. Self-diffusion coefficient

Figure 4 illustrates the variations of self-diffusion coefficients for four elements (Mg, Si, O, Fe) in $Mg_{0.9}Fe_{0.1}SiO_3$ as a function of pressures. For O elements at 4000 K, the diffusion coefficients exhibit a relatively complex response to pressure. The diffusion coefficient of O is 2.02×10^{-8} m^2/s at 0 GPa. As pressure increases to 5 GPa, the diffusion coefficient decreases to 1.69×10^{-8} m^2/s. However, at 10 GPa, the diffusion coefficient decreases to 1.34×10^{-8} m^2/s, which is 33.6% lower than that at 0 GPa. This trend persists at 14 GPa, where the diffusion coefficient further reduces to 9.87×10^{-9} m^2/s. At 24 GPa, the diffusion coefficient speedily decreases to 7.29×10^{-9} m^2/s. A similar trend is observed for Si elements. At 4000 K and 0 GPa, the diffusion coefficient of Si is 1.54×10^{-8} m^2/s. As pressure increases to 5 GPa, the diffusion coefficient decreases to 1.23×10^{-8} m^2/s. However, at 10 GPa, the diffusion coefficient of Si decreases to 1.09×10^{-8} m^2/s. Like O element, the diffusion coefficient of Si exhibits a significant decrease at high pressure. The diffusion coefficient of Si is 6.68×10^{-9} m^2/s at 24 GPa, which reduces nearly by one order of magnitude compared to the value at 0 GPa.

For Mg and Fe elements at 4000 K, the self-diffusion coefficients also show distinct pressure dependencies. At 0 GPa, the diffusion coefficient of Mg is 4.04×10^{-8} m^2/s, and that of Fe is 3.82×10^{-8} m^2/s. As pressure increases to 5 GPa, the diffusion coefficient of Mg decreases to 2.69×10^{-8} m^2/s, while Fe's diffusion coefficient decreases to 2.58×10^{-8} m^2/s. At 24 GPa, the diffusion coefficient of Mg drops significantly to 1.13×10^{-8} m^2/s, and Fe's diffusion coefficient decreases to 1.07×10^{-8} m^2/s, showing a notable reduction compared to the value at 0 GPa.

The effect of temperature on the diffusion coefficients is in evidence. Figure 5 illustrates the variations of self-diffusion coefficients for four elements (Mg, Si, O, Fe) in $Mg_{0.9}Fe_{0.1}SiO_3$ melts as a function of temperatures. For example, the diffusion coefficient of O under 24 GPa increases from 5.05×10^{-11} m^2/s at 2000 K to 1.36×10^{-8} m^2/s at 5000 K. Similarly, the diffusion coefficient of Si under 24 GPa rises from 4.64×10^{11} m^2/s at 2000 K to 1.24×10^{-8} m^2/s at

5000 K, with an increase of about two orders of magnitude. In the case of Mg, the diffusion coefficient at 24 GPa also shows a notable increase, rising from 1.27×10^{-10} m^2/s at 2000 K to 1.92×10^{-8} m^2/s at 5000 K, which represents an increase of roughly one order of magnitude. Likewise, for the Fe element, as temperature increases from 2000 K to 5000 K under 24 GPa, the diffusion coefficient rises from 1.49×10^{-10} m^2/s to 2.03×10^{-8} m^2/s, showing a substantial increase of nearly two orders of magnitude.

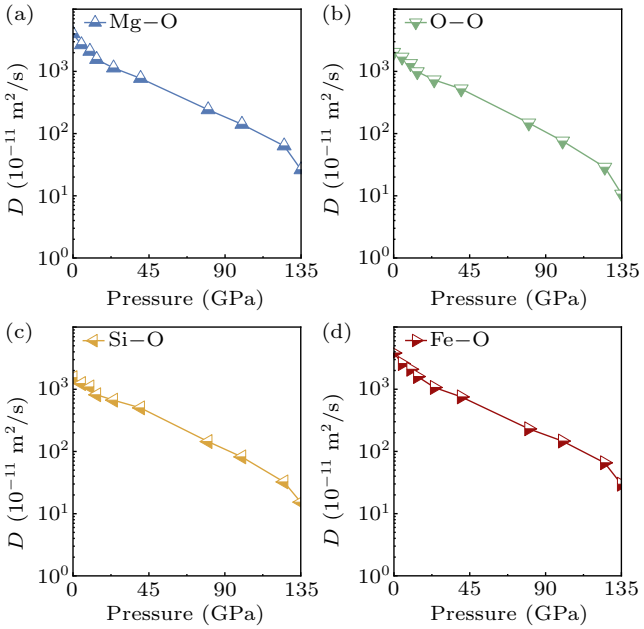


Fig. 4. The self-diffusion coefficients of $Mg_{0.9}Fe_{0.1}SiO_3$ melts at 4000 K. (a) Mg, (b) Si, (c) O, and (d) Fe.

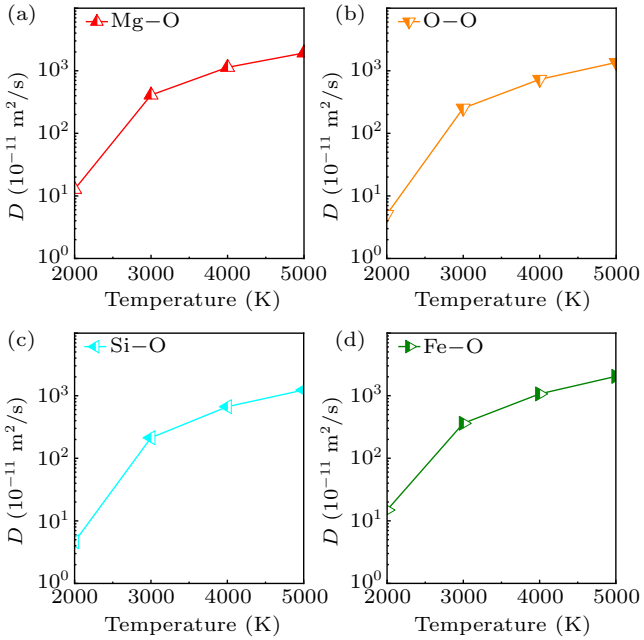


Fig. 5. The self-diffusion coefficients of $Mg_{0.9}Fe_{0.1}SiO_3$ melts at 24 GPa. (a) Mg, (b) Si, (c) O, and (d) Fe.

In general, the diffusion coefficients of O and Si elements exhibit similar trends with temperature and pressure. The elevated temperatures enhance diffusion coefficients, while high pressure conditions generally suppress diffusion. In particular, at 5000 K, the diffusion coefficients increase by several orders of magnitude, indicating the dominant influence of temperature on the diffusion process of $Mg_{0.9}Fe_{0.1}SiO_3$ melts.

3.2.2. Viscosity

To gain deeper insights into the influence of temperature and pressure on the viscosity of (Mg,Fe)SiO_3 melt, we have calculated the viscosity variations under different temperatures and pressures. The calculated viscosity of $MgSiO_3$ at 4000 K and 0 GPa in this work is approximately 9×10^{-3} Pa·s, which is similar to the value of 2×10^{-3} Pa·s reported in the work of Ghosh *et al.*[47] The results show that, as pressure increases, the viscosities of the (Mg,Fe)SiO_3 melt generally increase, especially at about the glass transition pressure point, where the viscosity increases remarkably.[44–46] This behavior may be attributed to the increase of the Si coordination numbers from four-fold to six-fold or even eight-fold under high pressure, leading to a denser melt structure that restricts particle diffusion.[47,48] In contrast, at the same pressure of 24 GPa, the viscosities of (Mg,Fe)SiO_3 decrease obviously as the temperature increases. For example, at 5000 K, the viscosity of (Mg,Fe)SiO_3 is reduced by about 2 orders of magnitude compared to that at 2000 K due to the enhanced ion mobility at higher temperatures, which increases fluidity and decreases viscosity. Overall, temperature exerts a more pronounced effect on viscosity than pressure.

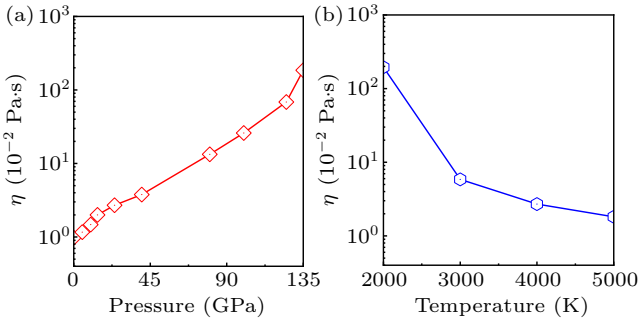


Fig. 6. The viscosities of (Mg,Fe)SiO_3 melts at different temperatures and pressures. (a) The viscosities of $Mg_{0.9}Fe_{0.1}SiO_3$ melts at 4000 K under different pressures. (b) The viscosities of $Mg_{0.9}Fe_{0.1}SiO_3$ melts under 24 GPa at different temperatures.

As shown in Fig. 6, the viscosity of $Mg_{0.9}Fe_{0.1}SiO_3$ exhibits notable variations under different temperatures and pressures. At 2000 K, the viscosity initially increases and then decreases with the increasing pressure. For instance, taking the viscosity of $Mg_{0.9}Fe_{0.1}SiO_3$ at 0 GPa as a reference, when the pressure increases to 5 GPa, the viscosity increases by only about 4.1%. At 10 GPa, the viscosity slightly decreases by 2.4%. When the pressure rises to 14 GPa, the viscosity increases by about one order of magnitude. Further increasing the pressure to 24 GPa results in a viscosity increase of about two orders of magnitude compared to that at 0 GPa, indicating

that pressure exhibits an enhanced effect on viscosity at lower temperatures.

At higher temperatures, the viscosity shows a clear decreasing trend. At 3000 K, the viscosity at 0 GPa decreases by 75.7% compared to that at 2000 K and 0 GPa. During the pressure increase from 0 GPa to 5 GPa, the viscosity decreases by 14.9%. However, the overall trend remains that viscosity diminishes markedly with the increasing temperature. For example, at 4000 K, the viscosity at 0 GPa is 90.1% lower than that at 2000 K and 0 GPa, and at 5000 K, it further decreases by 95.6%. This indicates that increasing temperature evidently enhances ion mobility, thereby improving melt fluidity and reducing the viscosity of $Mg_{0.9}Fe_{0.1}SiO_3$.

3.2.3. Electrical conductivity

The electrical conductivities of $Mg_{0.9}Fe_{0.1}SiO_3$ melts are calculated by Nernst–Einstein equation.[49–53] The calculated electrical conductivity of $MgSiO_3$ at 3000 K and 0 GPa is 423 S/m, compared to the value exceeding 200 S/m reported by Ghosh *et al.*[47] The variations of electrical conductivities of $Mg_{0.9}Fe_{0.1}SiO_3$ melt at different temperatures and pressures are shown in Fig. 7. As illustrated in Fig. 7, the electrical conductivities of $Mg_{0.9}Fe_{0.1}SiO_3$ melt exhibit an increasing trend under pressures ranging from 0 to 5 GPa.

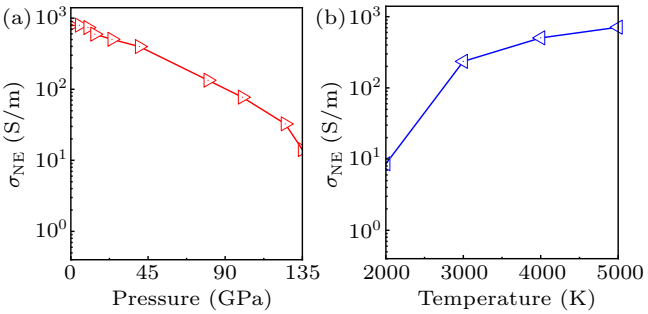


Fig. 7. The electrical conductivities of $Mg_{0.9}Fe_{0.1}SiO_3$ melts at different temperatures and pressures. (a) The electrical conductivities of $Mg_{0.9}Fe_{0.1}SiO_3$ melts at 4000 K under different pressures. (b) The electrical conductivities of $Mg_{0.9}Fe_{0.1}SiO_3$ melts under 24 GPa at different temperatures.

However, when the pressure exceeds 5 GPa, the electrical conductivities start to decrease with the increase of pressure, likely due to a compression effect on the ionic migration pathways and the freedom of movement, which restricts ion transport and results in decreased conductivity. The discrepancies between the maximum and minimum electrical conductivities are about two orders of magnitude, which are 502 S/m at 24 GPa and 77 S/m at 100 GPa. In contrast, temperature shows an even more pronounced effect on electrical conductivities of $Mg_{0.9}Fe_{0.1}SiO_3$ melt. The electrical conductivities increase monotonically with temperature. For example, at 0 GPa, the electrical conductivity rises from 129 S/m at 2000 K to 407 S/m at 3000 K, then to 787 S/m at 4000 K, and finally reaches the peak value of 1195 S/m at 5000 K. This behavior demonstrates that the increase of temperature enhances the ionic mobility, leading to a substantial increase in electrical conductivity of $Mg_{0.9}Fe_{0.1}SiO_3$ melt.

3.2.4. The effect of iron dopant

To explore the effect of Fe^{2+} doping on the structural and transport properties, we have calculated the microstructures, self-diffusion coefficients, viscosities, and electrical conductivities of $(Mg,Fe)SiO_3$ with varying iron contents under 24 GPa and 4000 K. The Fe^{2+} dopant induces notable modifications in bond lengths and coordination environments of $(Mg,Fe)SiO_3$. As Fe^{2+} content increases, the Fe–O bond lengths slightly elongate, ranging from 1.991 Å in $Mg_{0.95}Fe_{0.05}SiO_3$ to 2.013 Å in $Mg_{0.85}Fe_{0.15}SiO_3$. In contrast, the Mg–O bond length remains relatively stable at about 1.950 Å, while the Si–O bond length increases slightly, from 1.617 Å in $MgSiO_3$ to 1.639 Å in $Mg_{0.85}Fe_{0.15}SiO_3$. These changes indicate that Fe^{2+} doping introduces localized structural distortions around O atoms.

The Fe^{2+} primarily forms FeO_5 and FeO_6 coordination complexes. At high Fe^{2+} concentrations, for instance $Mg_{0.9}Fe_{0.1}SiO_3$ a small fraction ($\sim$ 15% Fe^{2+}) adopts FeO_7 coordination. Additionally, Fe^{2+} doping slightly affects Mg–O coordination, increasing the proportions of MgO_5 and MgO_6 complexes. These structural adjustments are attributed to the larger ionic radius of Fe^{2+} compared to Mg^{2+} and the higher polarizability of Fe^{2+}, which causes the rearrangement of nearby O atoms and leads to local structural changes. For Si–O coordination, the addition of Fe^{2+} causes a shift in the distribution of Si–O coordination numbers. The dominant coordinated complexes in $Mg_{0.9}Fe_{0.1}SiO_3$ are SiO_4 ($\sim$ 43%) and SiO_5 ($\sim$ 43%), with a smaller proportion adopting SiO_6 ($\sim$ 13%). These changes reflect a slight redistribution of Mg and Si coordination environments in $(Mg,Fe)SiO_3$ due to the presence of Fe^{2+} dopant.

The self-diffusion coefficients of all elements show minimal variations with increasing Fe^{2+} content. The diffusion coefficient of O remains relatively stable, increasing slightly from 6.96×10^{-9} m^2/s in $Mg_{0.95}Fe_{0.05}SiO_3$ to 7.30×10^{-9} m^2/s in $Mg_{0.85}Fe_{0.15}SiO_3$. Similarly, the diffusion coefficient of Si varies from 6.24×10^{-9} m^2/s in $Mg_{0.95}Fe_{0.05}SiO_3$ to 6.68×10^{-9} m^2/s in $Mg_{0.85}Fe_{0.15}SiO_3$. The diffusion coefficients of Mg are almost unchanged, which are 1.13×10^{-8} m^2 /s for $(Mg_{0.95},Fe_{0.05})SiO_3$ and 1.07×10^{-8} m^2/s for $Mg_{0.85}Fe_{0.15}SiO_3$. These results suggest that the impacts of Fe^{2+} doping on the self-diffusion coefficients of $(Mg,Fe)SiO_3$ are limited due to the relatively low concentration of Fe^{2+} dopant.

The viscosity of the $(Mg,Fe)SiO_3$ melt shows minor changes with increasing Fe^{2+} content. The viscosity of pure

$MgSiO_3$ is 2.77×10^{-2} Pa·s, increasing slightly to 2.83×10^{-2} Pa·s for $Mg_{0.95}Fe_{0.05}SiO_3$ and decreasing little to 2.71×10^{-2} Pa·s for $Mg_{0.9}Fe_{0.1}SiO_3$. At the highest Fe^{2+} content, $Mg_{0.85}Fe_{0.15}SiO_3$, the viscosity decreases further to 2.70×10^{-2} Pa·s. These minor variations can be attributed to the polarizing effects of Fe^{2+} which moderately affect the fluidity of (Mg,Fe)SiO_3 melt. However, the Fe^{2+} are localized, resulting in relatively stable viscosity of (Mg,Fe)SiO_3 melt with different doping concentrations.

The electrical conductivities of (Mg,Fe)SiO_3 melts are sensitive to Fe^{2+} contents. For $MgSiO_3$, the electrical conductivity is 492 S/m, which slightly decreases to 480 S/m for $Mg_{0.95}Fe_{0.05}SiO_3$. With increasing Fe^{2+} content, the electrical conductivity rises to 502.45 S/m for $Mg_{0.9}Fe_{0.1}SiO_3$ and stabilizes at 497 S/m for $Mg_{0.85}Fe_{0.15}SiO_3$. The enhancement in electrical conductivity with Fe^{2+} doping may be due to the introduction of additional mobile charge carriers, which improve charge transport within the (Mg,Fe)SiO_3 melts.

4. Conclusion

In summary, we have systematically studied the structural and transport properties of (Mg,Fe)SiO_3 under high temperature and high pressure using molecular dynamics simulations. The results reveal that the coordination environments of Si in (Mg,Fe)SiO_3 are mainly four-fold coordination under low pressure conditions, transitioning to six-fold and eventually eight-fold coordination at high pressure. This evolution in coordination environments of Si directly influences the diffusion coefficients, viscosities, and electrical conductivities of (Mg,Fe)SiO_3. Normally, the increased pressure obviously reduces the diffusion coefficients, while increasing the viscosities of (Mg,Fe)SiO_3. In contrast, higher temperature slightly decreases the viscosities, while markedly enhancing the diffusion coefficients and electrical conductivities of (Mg,Fe)SiO_3. Furthermore, Fe^{2+} doping promotes the diffusion of Si and O, reduces viscosities, and improves electrical conductivities of (Mg,Fe)SiO_3. These findings offer insights into the structural and transport properties of (Mg,Fe)SiO_3 under extreme conditions, which are important for advancing our understanding of the intricate geological processes occurring within the Earth's mantle.

Acknowledgments

Project supported by the National Natural Science Foundation of China (Grant Nos. 12174352 and 12111530103) and the Fundamental Research Funds for the Central Universities, China University of Geosciences (Wuhan) (Grant No. G1323523065).

References

[1] Zhou L, Zhou L X, Hardy J R, *et al.* 1998 *Chin. Phys. Lett.* **15** 444
[2] Deng L W, Zhao J J, Ji G F, *et al.* 2006 *Chin. Phys. Lett.* **23** 2334
[3] Yang F, Zeng Q, Chen B, *et al.* 2022 *Chin. Phys. Lett.* **39** 116301
[4] Elkins-Tanton L T and Hager B H 2005 *Earth Planet. Sci. Lett.* **239** 219
[5] Abe Y and Matsui T 1986 *J. Geophys. Res-sol. Ea.* **91** E291
[6] Canup R M 2012 *Science* **338** 1052
[7] Karki B B and Stixrude L P 2010 *Science* **328** 740
[8] Labrosse S, Hernlund J W and Coltice N 2007 *Nature* **450** 866
[9] Zheng Y F 2019 *Geosci. Front.* **10** 1223
[10] Koppers A A P, Becker T W, Jackson M G, *et al.* 2021 *Nat. Rev. Earth Env.* **2** 382
[11] Shim S H, Duffy T S and Shen G 2001 *Science* **293** 2437
[12] Zhang Z, Stixrude L and Brodholt J 2013 *Earth Planet. Sci. Lett.* **2013** 1
[13] Frost D J and McCammon C A 2008 *Annu. Rev. Earth Planet. Sci.* **36** 389
[14] Xu S, Lin J F and Morgan D 2017 *J. Geophys. Res-sol. Ea.* **122** 1074
[15] Dorfman S M, Potapkin V, Lv M, *et al.* 2020 *Am. Mineral.* **105** 1030
[16] Wang D, Wu Z and Deng X 2023 *Earth Planet. Sci. Lett.* **621** 118368
[17] Ni H, Hui H and Steinle-Neumann G 2015 *Rev. Geophys.* **53** 715
[18] Mosenfelder J L, Asimow P D, Frost D J, *et al.* 2009 *J. Geophys. Res-sol. Ea.* **114** B1
[19] Karki B B, Ghosh D B, Maharjan C, *et al.* 2018 *Geophys. Res. Lett.* **45** 3959
[20] Xie L, Yoneda A, Yamazaki D, *et al.* 2020 *Nat. Commun.* **11** 548
[21] Ghosh D B and Karki B B 2011 *Geochim. Cosmochim. Acta* **75** 4591
[22] Laumonier M, Scaillet B, Arbaret L, *et al.* 2015 *Chem. Geol.* **418** 158
[23] Sun Y, Zhou H, Yin K, *et al.* 2018 *J. Geophys. Res.* **123** 3667
[24] Liebske C, Schmickler B, Terasaki H, *et al.* 2005 *Earth Planet. Sci. Lett.* **240** 589
[25] Reid J E, Suzuki A, Funakoshi K I, *et al.* 2003 *Phys. Earth Planet. In.* **139** 45
[26] Cochain B, Sanloup C, Leroy C, *et al.* 2017 *Geophys. Res. Lett.* **44** 818
[27] Marsh B D 2007 *J. Am. Ceram. Soc.* **90** 746
[28] Guo Z S, Xing D, Xi X Y, *et al.* 2022 *Adv. Fiber Mater.* **4** 923
[29] Guo Z S, Xing D, Xi X Y, *et al.* 2024 *iScience* **27** 8
[30] Holzapfel C, Rubie D C, Frost D J, *et al.* 2005 *Science* **309** 1707
[31] Kavner A, Li X and Jeanloz R 1995 *Geophys. Res. Lett.* **22** 3103
[32] Chen M, Raghunath S and Zhao B 2014 *Metall. Mater. Trans. B* **45** 58
[33] Wan J T, Duffy T S, Scandolo S, *et al.* 2007 *J. Geophys. Res.* **112** B3
[34] Thompson A P, Aktulga H M, Berger R, *et al.* 2002 *Comput. Phys. Commun.* **271** 108171
[35] Hoover W G 1985 *Phys. Rev. A* **31** 1695
[36] Nosé S 1984 *J. Chem. Phys.* **81** 511
[37] Hoover W G 1986 *Phys. Rev. A* **34** 2499
[38] Van Beest B W H, Kramer G J, and Van Santen R A 1990 *Phys. Rev. Lett.* **64** 1955
[39] Guillot B and Sator N 2007 *Geochim. Cosmochim. Ac.* **71** 1249
[40] Guillot B and Sator N 2007 *Geochim. Cosmochim. Ac.* **71** 4538
[41] Solomatova N V and Caracas R 2019 *J. Geophys. Res-sol. Ea.* **124** 11232
[42] Brown G E, Farges F, Calas G, *et al.* 1995 *Rev. Mineral.* **32** 317
[43] Cormier L, Gaskell P H, Calas G, *et al.* 1998 *Phys. Rev. B* **58** 11322
[44] Schober H R and Peng H L 2016 *Phys. Rev. E* **93** 052607
[45] Ould-Kaddour F and Levesque D 2000 *Phys. Rev. E* **63** 011205
[46] Voronel A, Veliyulin E, Machavariani V S, *et al.* 1998 *Phys. Rev. Lett.* **80** 2630
[47] Ghosh D B and Karki B B 2017 *Sci. Adv.* **3** e1701840
[48] Müller-Plathe F 1994 *Acta Polym. Sin.* **45** 259
[49] Petrowsky M and Frech R 2010 *J. Phys. Chem. B* **114** 8600
[50] Novella D, Jacobsen B, Weber P K, *et al.* 2017 *Sci. Rep.* **7** 5344
[51] Liu Y, Fan Q, Yang J, *et al.* 2022 *Chin. Phys. Lett.* **39** 127403
[52] Zhang R, Guo R, Li Q, *et al.* 2024 *Chin. Phys. B* **33** 108103
[53] Chen Q, Wu J, Chen T, *et al.* 2022 *Chin. Phys. B* **31** 056201